Nickel oxide immobilized on the carbonized eggshell membrane for electrochemical detection of urea

Shun Lu[a,e*], Zhengrong Gu[a,Z], Matthew Hummel[a], Yue Zhou[b], Keliang Wang[c], Ben Bin Xu[e], Yucheng Wang[e], Yifan Li[e], Xueqiang Qi[d,Z], Xiaoteng Liu[e,Z]

a Department of Agricultural and Biosystems Engineering, South Dakota State University, Brookings 57007, SD, USA
b Department of Electrical Engineering and Computer Science, South Dakota State University, Brookings 57007, SD, USA
c Department of Electrical Engineering and Computer Engineering & Department of Chemical Engineering and Materials Science, Michigan State University, East Lansing, MI, 48824, USA
d College of Chemistry and Chemical Engineering, Chongqing University of Technology, Chongqing, 400054, China
e Department of Mechanical & Construction Engineering, Faculty of Engineering and Environment, Northumbria University, Newcastle upon Tyne, NE1 8ST, UK

[Z]Corresponding Authors: Zhengrong.Gu@sdstate.edu (Z. Gu), xqqi@cqut.edu.cn (X. Qi) and terence.liu@northumbria.ac.uk (X. Liu)

[*]Electrochemical Society Student Member

Abstract

Urea oxidation reaction (UOR) has been known as a viable method for renal/liver disease diagnostic detection. Here, we reported a three-dimensional (3D) nickel oxide nanoparticles dressed carbonized eggshell membrane (3D NiO/c-ESM) as a modified electrode toward urea detection. Several common physical measurements were employed to confirm its structural and morphological information. NiO/*c*-ESM modified electrode exhibits an outstanding performance for urea determination with a linear range from 0.05 to 2.5 mM, and limit detection of ~20 μM (3σ). This work offered a green approach for introducing 3D nanostructure through employing biowaste ESMs as templates, providing a typical example for producing new value-added nanomaterials with urea detection.

Keyword: urea oxidation, nickel oxide, eggshell membrane, electrochemical sensor.

Introduction

Urea ($CO(NH_2)_2$) is the main nitrogen-containing substance from the urine of human/animal, which is also an effective and critical indicator in evaluating various metabolic disorders.(1-3) Urea can decompose naturally to toxic ammonia and nitrates permeating into groundwater, then cause environmental problems and even health issues.(4-6) Therefore, the detection of urea concentration and decomposition of urea-rich sewage is vitally important in the human health and environmental industries.(7-12) The electrochemical urea oxidation reaction (UOR, $CO(NH_2)_2 + 6OH^- \rightarrow N_2 + CO_2 + 5H_2O + 6e^-$) was developed recent years that making urea electrolysis easier, consuming much less energy (0.37 V) compared to the electrochemical process of water splitting (1.23 V) in terms of hydrogen production (3, 13), and also utilizing this reaction for electrochemical sensor towards urea.(14-16) Gupta and co-authors reported several electrochemical sensors toward metal ions(17-20), uric acid(21), dexamethasone(22), and corticosteroid triamcinolone(23) via voltammetry and amperometry. Electrochemical measurements are regarded as favorable for quantitative analysis due to their fast response and high sensitivity.(17, 24-32)

Eggshell membrane (ESM), is derived from the eggshells of industrial egg processors are regarded as biowaste.(33) ESM is mainly comprised proteins which form interwoven fibrous structures and has a strong adsorption capacity to bind and confine metal ions.(34) Besides, it also can keep stable structure in aqueous and alcoholic media and undergo pyrolysis.(35) Interestingly, these biowaste ESM as support could effectively immobilize and disperse nanoparticles that the reason of the unique three dimensional (3D) porous network and plenty of functional groups such as amines, amides and carboxylic surface functional groups and the resulting nanocomposites have been reported to display enhanced catalysis and sensing activity such as $CoFe_2O_4$@C(36), NiO-Ni@C(37), FeS@C(38) and Au network(39), etc.(40, 41) The unique network structure of ESM composed of biomacromolecular fibers provides a novel template for the functional groups, also with superior porosity and specific surface area, which can offer multiple transport pathways for both electrons and ions.

In this work, ESM was utilized here as a bio-template for the rational design of the electrode material, furthermore, nickel ions can be absorbed on its surface to form the precursor ($Ni(OH)_2$/ESM). Consequently, we reported an integrated 3D network composed of NiO nanoparticles anchoring on the carbonized ESM using a mixed method of hydrothermal and pyrolysis. The NiO nanoparticles anchored 3D carbonized network of the catalyst provides more catalytic active sites and enables easy access of reactants to the catalyst surfaces. Experimental results confirmed synergetic effect between NiO nanoparticles and the *c*-ESM with higher exposed active sites, and faster electron transport, ensuring its superior performance of urea detection. It is worth mentioning that the biowaste ESM can convert into a useful support for the as-prepared sensor. This work also shed light on the great potential for further applications in “trash to treasure”.

Experimental

Chemical and reagents. All reagents were of analytical reagent grade, purchased from Fisher Scientific Co LLC and Alfa Aesar Chemical Reagent Co, Ltd., and used as received without further purification. Fresh eggs were bought from the local market.

Preparation of c-ESM. Eggshell membrane was processed first by removing the eggshell, then rinsed with large amounts of de-ionized water (DIW, 18.4 MΩ cm^{-1}, Milli-Q) to remove excess yolk and egg white and dried at room temperature, followed by calcination at 500 °C for 2 h under a heating rate of 10 °C/min in N_2 atmosphere. The carbonized ESM (named as *c*-ESM) was collected after washing with DIW and drying at room temperature.

Synthesis of 3D NiO/C nanocomposites. Briefly, 3D NiO/C nanocomposites were fabricated through a simple two-step method, as illustrated in **Scheme 1**. (i) eggshell with a top hole was rinsed with large amounts of DIW in order to obtain a clean container, then 0.1 M $Ni(NO_3)_2$ solution was transferred into a cleaned eggshell, and 20 mL urea solution was added into a beaker. (ii) eggshell with nickel nitrate aqueous was immersed into urea solution in a beaker and maintained at 70 ℃ for 6 h. In this process, a large amount of Ni^{2+} ions were absorbed on the microporous network of ESM, and hydroxyl (OH^-) ions were producing from urea while heating. (iii) the reaction system was cooled to room temperature naturally, and the $Ni(OH)_2$/ESM precursor was peeled from eggshell reactor. The stripped precursor was rinsed thoroughly with DIW. (iv) $Ni(OH)_2$/ESM was calcined at 500 ℃ for 2 h in the protection of N_2, the final product (NiO/c-ESM) was then cooled to room temperature with N_2 protection. The resulting black powder of 3D NiO/c-ESM nanocomposites was collected for further use. Pure NiO particles were synthesized with the same procedure except for the absence of ESM as for comparison.

Physical characterization. Structural information of the samples was carried out on X-ray diffraction (XRD, Rigaku, λ= 1.5418 Å). The scanning electron microscopy (SEM, Hitachi S-3400N) was used to observe the surface morphologies of the as-prepared samples. Transmission electron microscopy (TEM, JEOL JEM-2100F) and high-resolution transmission electron microscope (HRTEM) were operated under an accelerating voltage of 200 kV. STEM-EDS (Oxford) was used for confirming the elements of the as-prepared sample.

Electrochemical characterizations. All electrochemical tests were carried out on an electrochemical workstation (CHI 760E, Austin, Texas) with a typical three-electrode system. A catalyst-modified glassy carbon electrode (3 mm in diameter), Pt foil, and Ag/AgCl with saturated KCl solution were selected as the working electrode, counter electrode, and reference electrode, respectively. The details of electrode preparation and electrochemical setup were set up according to our previously reported. The loading mass of the as-prepared catalyst (4 μL, 1.33 mg mL^{-1}) on the electrode surface is *ca.* 0.075 mg cm^{-2}. All electrochemical tests were also performed with the same setting as previous reported(30). Square wave voltammetry (SWV) was chosen as primary technique for detection. Here, all tests were performed at 25 ℃ and all potentials were converted versus a reversible hydrogen electrode (RHE) based on the Nernst equation: ($E_{RHE} = E_{Ag/AgCl} + 0.059 \times pH + 0.21$ V, 25℃) unless otherwise specified.

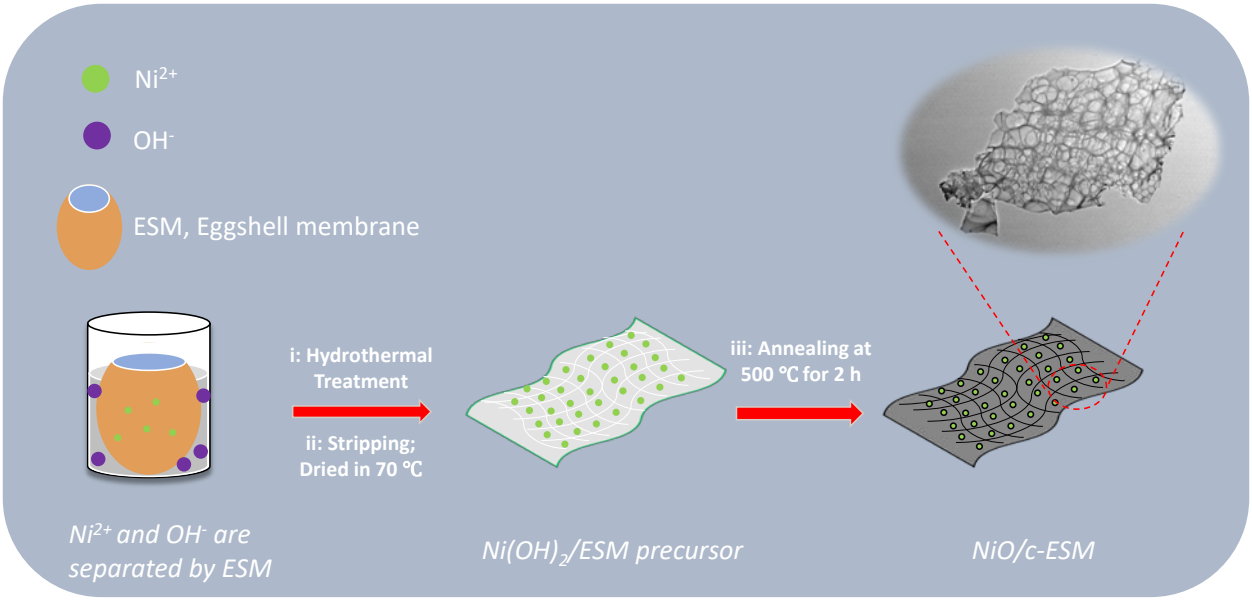

Scheme 1. Illustration of synthesis procedure of NiO/*c*-ESM

Results and Discussion

3D NiO/*c*-ESM nanocomposites were prepared through a simple two-step method, as schematically demonstrated in **Scheme 1**. The mechanism for preparation of NiO/*c*-ESM nanocomposites can be expressed as follows (**Equation.1-4**):

$$CO(NH_2)_2 + H_2O \rightarrow CO_2 + NH_3 \quad (1)$$

$$NH_3 + H_2O \rightarrow NH_4^+ + OH^- \quad (2)$$

$$Ni^{2+} + 2OH^- + ESM \rightarrow Ni(OH)_2/ESM \quad (3)$$

$$Ni(OH)_{2_{ESM}} \xrightarrow{carbonization} NiO_{c-ESM} + H_2O \quad (4)$$

X-ray diffraction has been applied to study the structural information of the as-prepared samples. **Fig. 1a** reveals that the XRD pattern of NiO/*c*-ESM nanocomposites. A series of typical diffraction peaks (2θ: 37.2°, 43.2°, 62.8°) corresponding to (111), (200) and (220) crystal planes, indicating the formation of pure nickel oxide (JCPDS No.47-1049). Furthermore, the broad peak at 2θ of 24.8° corresponds to an experimental *d* spacing of 3.37 Å indicating presence of graphite-like carbon (JCPDS No. 41-1487). **Fig. 1b** presents that the SEM image of NiO/*c*-ESM nanocomposites with an obvious network-like morphology. TEM images (**Fig. 1c-d**) further confirmed the *c*-ESM and NiO/*c*-ESM with the crosslink-like morphological feature and its pore lateral size of ~200 nm, while the transparent characteristic of the *c*-ESM indicates its ultrathin thickness. In the **Fig. 1e**, NiO nanoparticles (size: ~15 nm in diameter) were anchored on the surface of c-ESM with high and even dispersion identified by TEM observation, their morphology appears good dispersion. **Fig. 1f** presents the nitrogen adsorption/desorption isotherm and pore size distribution of NiO/*c*-ESM nanocomposites. The BET specific surface areas of NiO/*c*-ESM was found

to be 79.6 m2 g^{-1}. The isotherms resemble to the type IV classification. The hysteresis loop starts at the relative pressure (P/P_0) of about 0.45 and expends almost to 1, indicating that NiO nanoparticles are mesoporous, which is associated with the c-ESM with the filling of the mesopores. The inset of **Fig. 1f** also confirmed NiO nanoparticles is with the average diameter of ~15 nm, keep consistent with TEM observation.

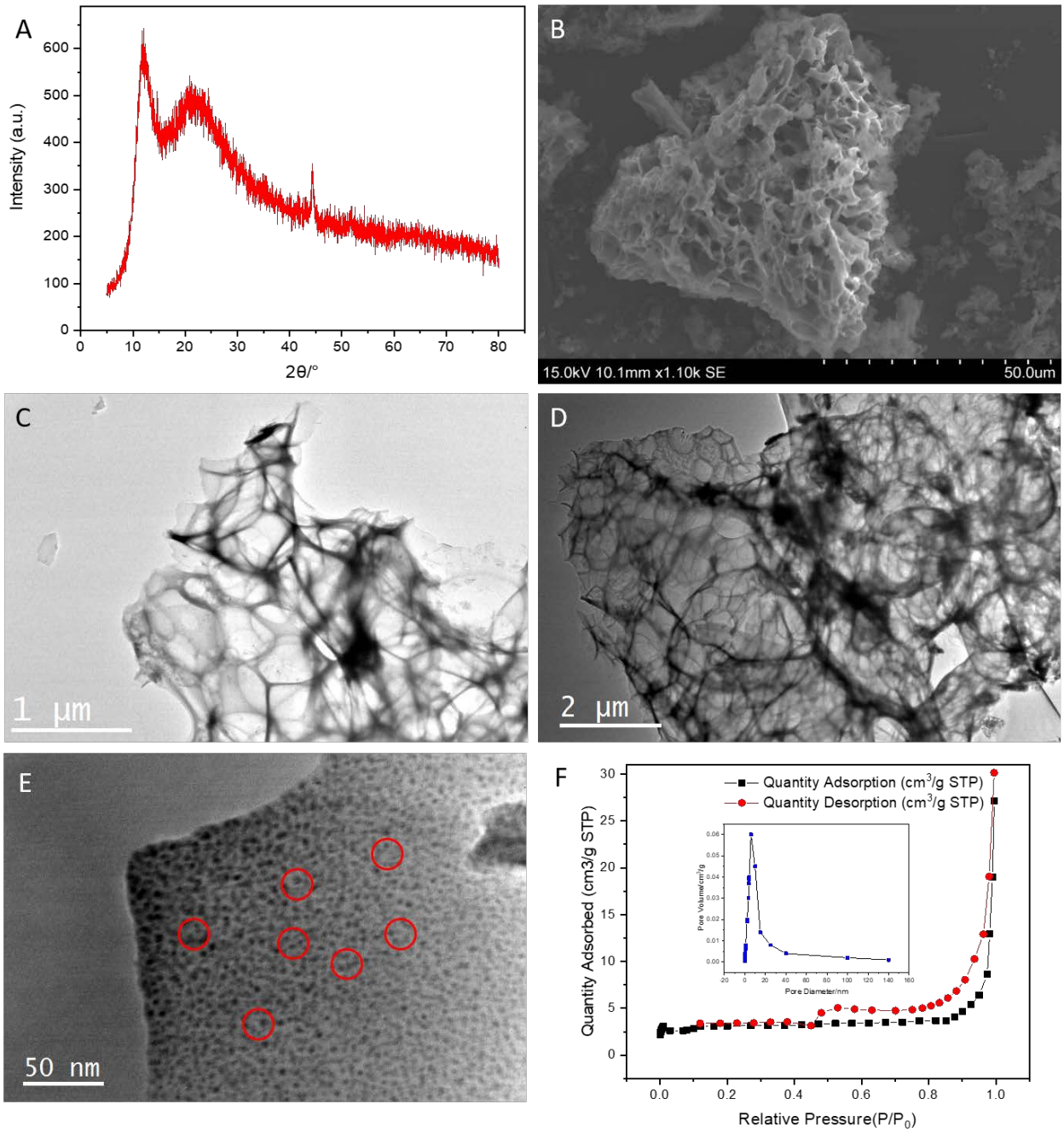

Figure 1. (a) XRD pattern and (b) SEM image of NiO/c-ESM, TEM image of (c) *c*-ESM and (d) NiO/c-ESM, (e) selected area TEM from (d), (f) BET analysis of NiO/*c*-ESM, inset: pore size distribution of NiO/*c*-ESM corresponding to (f).

To further verify the surface topology of the 3D NiO/*c*-ESM nanocomposites, the elemental composition is illustrated by using scanning transmission electron microscopy-energy dispersive X-ray spectroscopy (STEM-EDX) mapping. **Fig. 2** presents EDX results of the 3D NiO/*c*-ESM nanocomposites, they prove that the as-prepared nanocomposite is mainly composed of Ni, O and C (here, the existence of Ca, Cr, and Cu is caused by the Cu mesh), and STEM-EDS mapping in **Fig. 2c** indicates that these elements are dispersed uniformly. Based on the above observation (**Fig. 1-2**), it can be proposed that nickel ions are adsorbed on the inner surface of ESM during the preparation of NiO/*c*-ESM nanocomposites, and hydroxyl ion released from urea reacted with the adsorbed nickel ions, this kind of hybrid precursor kept the network-like structure synergistically stable that prevents the shrinkage caused by thermal annealing.(37, 42) Therefore, the surface of NiO/*c*-ESM nanocomposites become an obvious network-like morphology with plenty of porous structure.

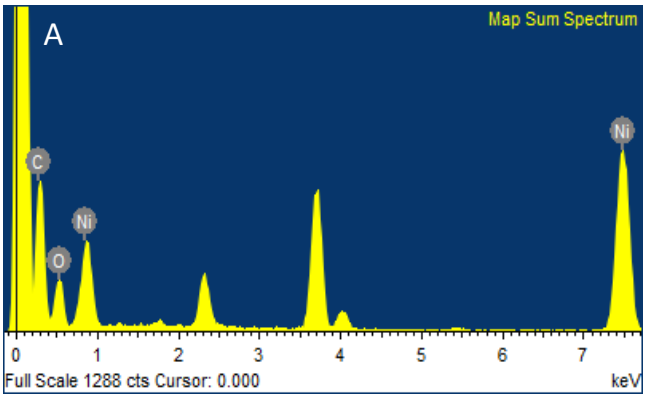

B

Element	Weight%	Atomic%
C K	0.30	1.48
O K	0.11	0.42
Ca K	0.16	0.24
Cr K	0.45	0.51
Ni K	68.13	68.64
Cu K	30.85	28.71
Totals	100.00	

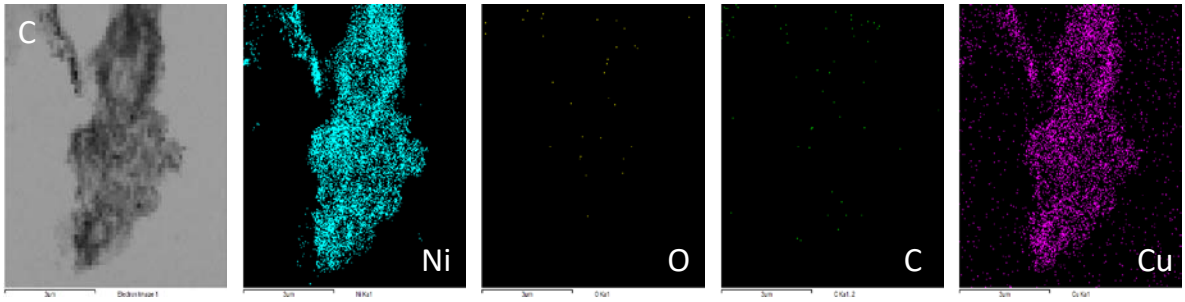

Figure 2. (a) EDX spectra, (b) element contents and (c) STEM-EDX mapping images of NiO/*c*-ESM.

The electrocatalytic performance of NiO/*c*-ESM toward urea is evaluated by CV employing a typical three-electrode testing system. **Fig. 3** displays CVs of NiO/*c*-ESM in 1.0 M KOH solution in the absence and presence of 0.33 M urea, *c*-ESM was also tested for comparison. It could be seen that after addition of 0.33 M urea, there was almost no change for *c*-ESM in terms of current density. In sharp contrast, both NiO/*c*-ESM has obvious increase in oxidation peak current response due to the oxidation of Ni(II) to Ni(III) in the presence of OH^- ions for NiO nanoparticles anchored on the *c*-ESM.(11) The electrochemical kinetics of urea oxidation reaction was investigated in 1.0 M KOH solution containing 10 mM urea. (**Fig. 4a**). The relationship of peak current (I_p) and scan rate is investigated and compared (**Fig. 4b-c**). The peak current (I_p) plots were linearly proportional to the square root of scan rate with the higher correlation coefficients (R^2) of 0.998, suggesting a diffusion-controlled process (**Fig. 4c**). Furthermore, the results were

calculated from a straight-line plot of the current against minus square root of time (R^2 = 0.999), as shown in **Fig. 4d**, further verifying that the mechanism of oxidation of urea is a typical diffusion-controlled process.(43) Furthermore, the double layer capacitance (C_{dl}) has been studied to measure the electrochemical active surface area (EASA) of NiO/*c*-ESM and *c*-ESM modified electrodes (**Fig. 4e**) by CV technique in a narrow potential range (0.06-0.16 V, nonfaradaic zone) with a series of scan rates.(41, 44-46) After calculation, the EASA of NiO/*c*-ESM electrode is ~70.1 cm^2 higher than NiO electrode (50.3 cm^2) and *c*-ESM electrode (66.8 cm^2), suggesting that the effective active sites of NiO/*c*-ESM for urea oxidation is higher than that of *c*-ESM.(47) Electrochemical impedance spectroscopy (EIS) can be used to analysis the electron transfer process and impedance changes on the surface of the working electrode. **Fig. 4f** displays Nyquist plots of NiO/*c*-ESM and *c*-ESM under a loading potential of 1.45 V. The semicircular diameter of NiO/*c*-ESM (R_{ct}, 4.8 Ω) is smaller than that of NiO (R_{ct}, 8.2 Ω) and *c*-ESM (R_{ct}, 6.4 Ω), revealing that NiO/*c*-ESM has a better charge transfer during urea oxidation. Combined EASA calculation and EIS analysis, it demonstrated that NiO/*c*-ESM could be a potential electrode material for urea determination.

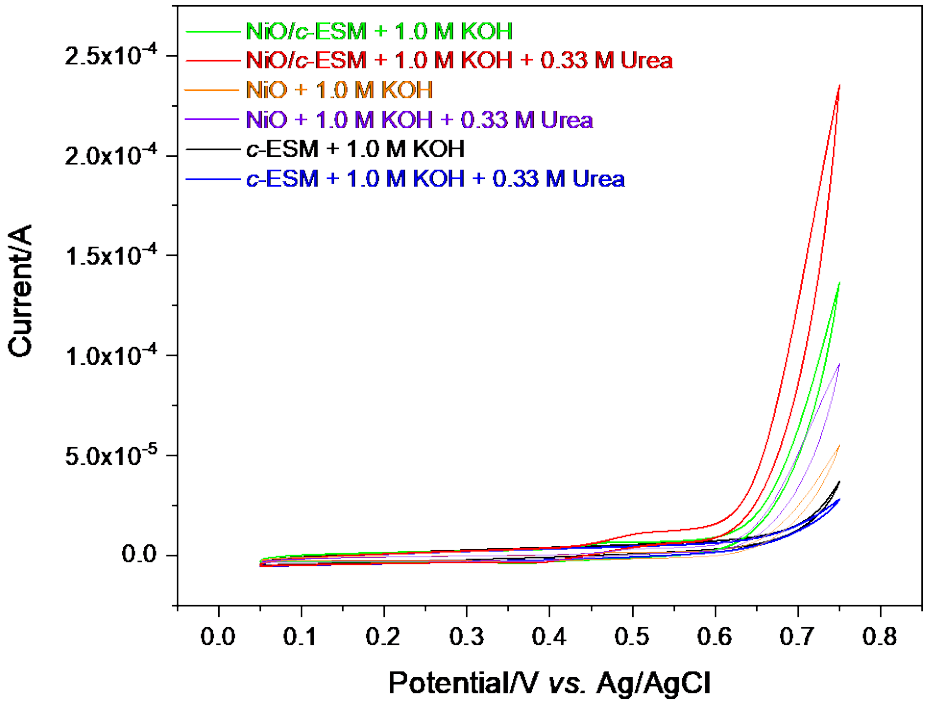

Figure 3. Cyclic voltammograms of NiO/*c*-ESM, NiO and *c*-ESM electrodes in the presence and absence of urea in 1.0 M KOH solution.

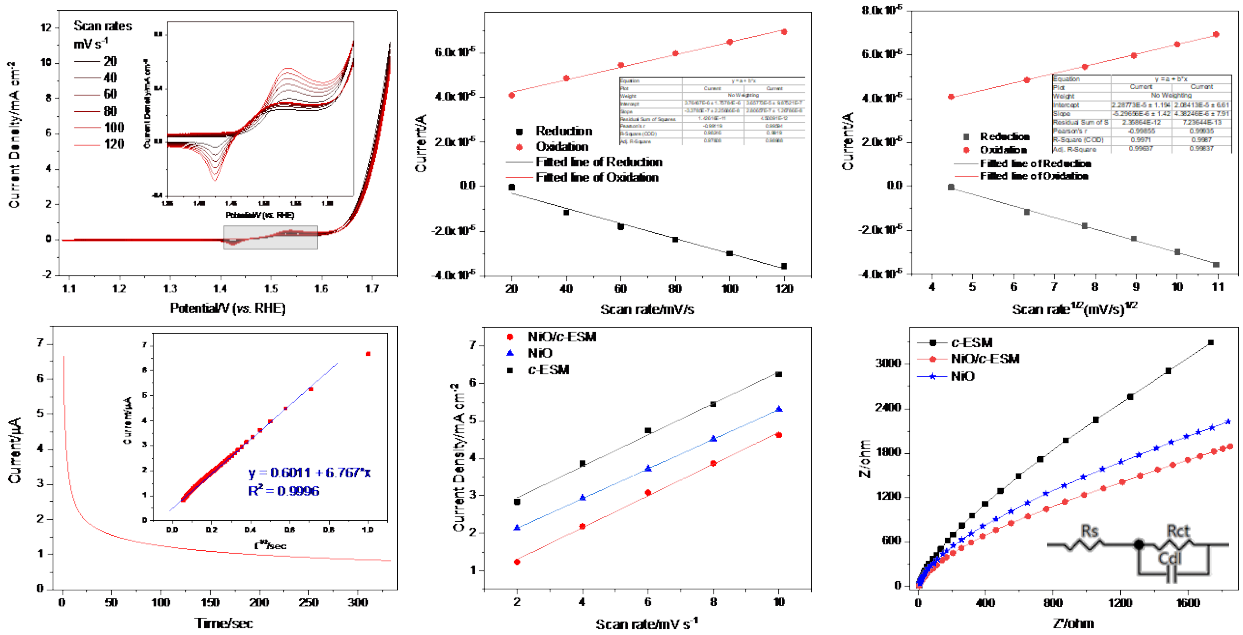

Figure 4. (a) Cyclic voltammograms of NiO/*c*-ESM in the presence of 10 mM urea in 1.0 M KOH at different scan rate (20-120 mV s^{-1}). Comparison of calibration plot of peak current *vs.* function of scan rate: (b) calibration plot of peak current *vs.* scan rate, (c) calibration plot of peak current *vs.* square root of scan rate. (d) Amperometric response of NiO/*c*-ESM in 1.0 M KOH with 2.0 mM of urea at potential of 1.45 V (*vs.* RHE), (inset) the plot of I *vs.* $t^{-1/2}$ derived from the amperometric curve. (e) The double layer capacitance of NiO/*c*-ESM, NiO and *c*-ESM electrode in a narrow potential range in 1.0 M KOH at different scan rates (10-50 mV s^{-1}). (f) Nyquist plots of NiO/*c*-ESM, NiO and *c*-ESM electrode in 1.0 M KOH.

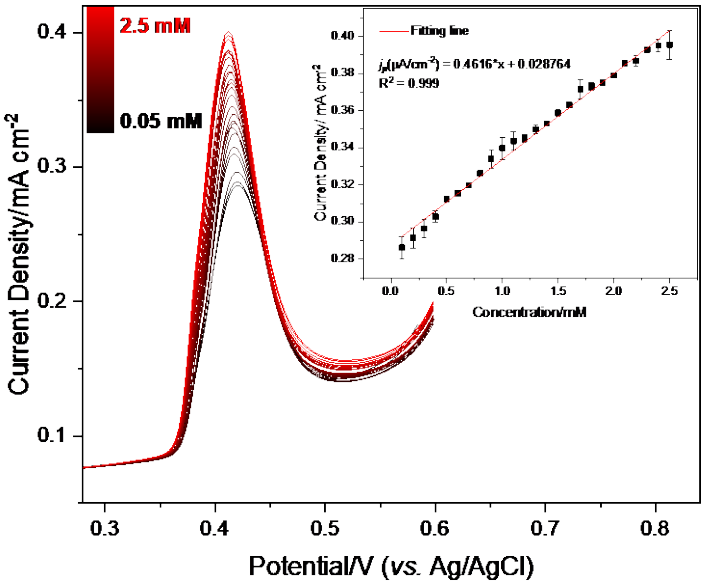

Figure 5. SWV curves of NiO/*c*-ESM to detect urea, inset: calibration curve of current density *vs.* urea concentration.

Square wave voltammetry (SWV) measurement was employed to record the response of NiO/*c*-ESM electrode with a series of urea concentrations. NiO(II) nanoparticles were oxidized to NiOOH(III) during the electrochemical process, then catalyzes the decomposition of urea. The functional Ni(III) which worked as active species, are simultaneously oxidized in the process. Benefiting from efficient electron transfer and reversible properties of the NiO nanoparticles and the porous *c*-ESM, the electrons generated from Ni(III)/Ni(II) redox are transferred to the surface of electrode. The NiO/*c*-ESM electrode presents a sensitivity of 0.462 $\mu A\ mM^{-1}\ cm^{-2}$ in the inset of **Fig. 5**. The results show that the limit of detection (LOD) is calculated to be ~20 μM from the SWV curves with the linear range from 0.05 to 2.5 mM with a correlation coefficient of 0.988 (3σ). This electrochemical sensor could achieve urea detection within 7 s (single sample). **Table 1** compares the data from the as-proposed sensor and other electrochemical sensors based on the urea determination, the as-proposed sensor exhibits lower LOD and superior sensitivity. The electrocatalytic activity and sensitivity toward urea for NiO/*c*-ESM could be attributed to the 3D network of *c*-ESM and NiO nanoparticles configuration of this electrode, exposing more active sites and facilitating enough transport of reactants and products.

Table 1. Sensing performance of the NiO/*c*-ESM electrode and recently reported electrochemical sensors towards urea

Electrode	Substrate	Linear range /mM	Sensitivity /$\mu A\ mM^{-1}\ cm^{-2}$	LOD/ μM	References
Ur-NiO	ITO[a]	0.99-11.50	22.39	N/A	(48)
MWCNT[b]	Silica	0.002-1.07	2.3	N/A	(49)
$NiCo_2O_4$/Graphene	ITO	0.06-0.30	166	5	(9)
Rh/Ur[c]	Platinum	0.1-1.75	1.85	50	(14)
NiO/Ur	ITO	0.83-16.65	21.3	830	(50)
MSA-QDs[d]	Optical method	0.01-120	N/A	10	(51)
NiO/*c*-ESM	Glassy carbon	0.05-2.5	0.462	~20	This work

a: Indium tin oxide; b: Multi-wall carbon nanotube; c: Urease; d: Quantum dots.

Selectivity and anti-interfering are another major index in evaluating the performance of electrochemical sensor. As displays in **Fig. 6a**, the current responses to different interfering species, such as Glucose (Glu), Na^+ ions, K^+ ions, and uric acid (UA) and the addition of urea was recorded. Those interfering species have similar electroactive behaviours that are easy to be oxidized, so their influences are non-negligible. It can be found that stair-like current response towards urea of the as-proposed electrode when successive added urea, whereas no obvious responses to the other interfering species are also obtained, suggesting the good selectivity of the electrochemical urea sensor in a diluted urea sample. The stability of NiO/*c*-ESM electrode was also examined. The parameters of CV tests could be remained at constant values upon 200 continuous CV scans over a potential window of 1.3 to 1.7 V in 1.0 M KOH (scan rate: 50 $mV\ s^{-1}$). **Fig. 6b** displays that the current assigned to urea oxidation is 76.4% of the initial value after 200 CV scans, thus suggesting good stability due to the stable structure between NiO nanoparticles and *c*-ESM.

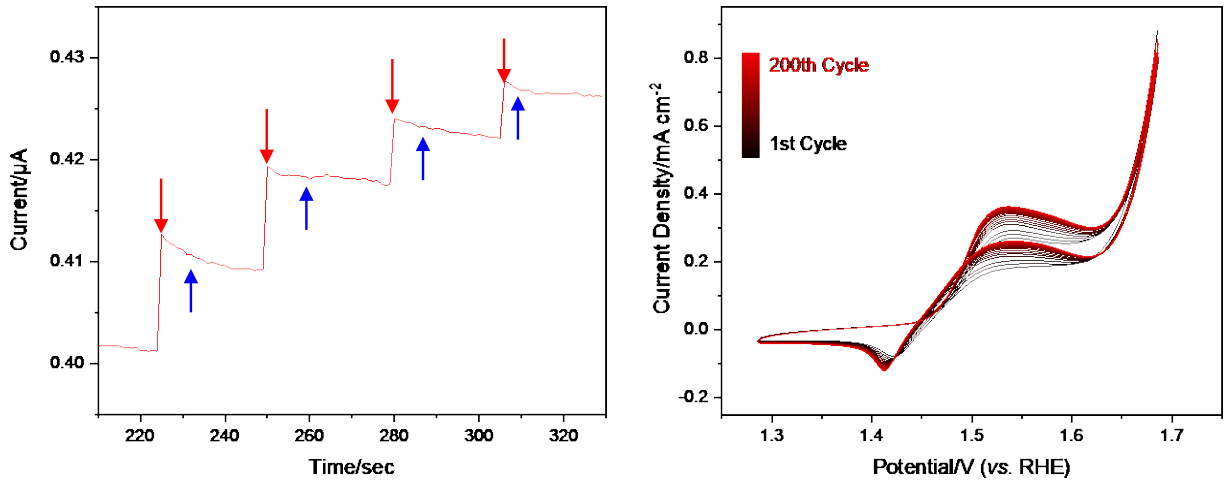

Figure 6. (a) The current responses to the addition of urea and different interfering species: 2.0 mM glucose, 2.0 mM Na^+, 2.0 mM K^+, 4.0 mM Cl^- and 2.0 mM uric acid. (d) Cycling stability tests of NiO/*c*-ESM in 1.0 M KOH with 0.33 M urea at a scan rate of 50 mV s^{-1}.

To evaluate the application of the NiO/*c*-ESM electrode, urea detection in real samples was examined. 10 μL tap water sample was spiked with 1.0 M KOH to obtain the test water sample, as shown in **Table 2**. The obtained recovery values for the determination of urea are between 92.8 and 105.2% for the test water samples. The relative standard deviation (RSD) value of <5% was obtained for three measurements of different spiked samples. Given the experimental results, this means the as-prepared NiO/*c*-ESM electrode has good selectivity toward urea determination.

Table 2. Determination of urea in alkaline buffer and tap water samples

Samples	Urea added /mM	Total found /mM (n = 3)	RSD% (n = 3)	Recoveries %
KOH buffer	0.01	0.0982	1.83	98.2
	1.0	1.021	1.92	102.1
	2.0	1.994	2.06	99.7
Tap water	0.01	0.0965	3.20	96.5
	1.0	0.928	1.76	92.8
	2.0	2.103	2.41	105.2

Conclusion

In summary, 3D NiO/*c*-ESM nanocomposites were experimentally prepared by a simple two-step method and employed as an electrocatalyst for urea detection. ESM as biowaste was used as precursor in this synthesis and make full use it. *c*-ESM with the large surface area provided a possible place for anchoring of the NiO nanoparticles uniformly. NiO/*c*-ESM modified electrode exhibits wider linear range (0.05 to 2.5 mM), low detection limit of ~20 μM (signal noise ratio is 3). Besides, the as-prepared electrochemical sensor presented good selectivity and satisfactory results in real sample application. In this study, 3D NiO/*c*-ESM nanocomposite electrode exhibits good performance and robust durability towards urea detection is attributed to the synergistic effect of more active sites from NiO nanoparticles and the carbonized porous eggshell membrane.

Acknowledgement

This work was supported by NASA EpsCor (No. NNX16AQ98A), USDA-NIFA Hatch (No. SD00H618-16, SD00R680-19 NC1194), NSF/EPSCoR (No. OIA-1849206, South Dakota 2D Materials for Biofilm Engineering, Science and Technology Center (2DBEST)), and the UK Engineering Physics and Science Research Council (Grant No. EP/S032886/1) for research support. S. Lu thanks the financial support from China Scholarship Council (CSC).

ORCID

Shun Lu https://orcid.org/0000-0003-4287-0779

References

1. Y. L. Liu, R. Liu, Y. Qin, Q. F. Qiu, Z. Chen, S. B. Cheng and W. H. Huang, *Anal Chem*, **90**, 13081 (2018).
2. S. E. Waisbren, A. L. Gropman, C. Members of the Urea Cycle Disorders and M. L. Batshaw, *J Inherit Metab Dis*, **39**, 573 (2016).
3. J.-Y. Zhang, T. He, M. Wang, R. Qi, Y. Yan, Z. Dong, H. Liu, H. Wang and B. Y. Xia, *Nano Energy*, **60**, 894 (2019).
4. S. G. Shen, B. B. Li, M. N. Li, J. M. Fan and Z. J. Zhao, *Desalin Water Treat*, **55**, 70 (2015).
5. Z. H. Yue, S. Y. Yao, Y. Z. Li, W. X. Zhu, W. T. Zhang, R. Wang, J. Wang, L. J. Huang, D. Y. Zhao and J. L. Wang, *Electrochim Acta*, **268**, 211 (2018).
6. E. Urbańczyk, A. Maciej, A. Stolarczyk, M. Basiaga and W. Simka, *Electrochim Acta*, **305**, 256 (2019).
7. D. Dutta, S. Chandra, A. K. Swain and D. Bahadur, *Anal Chem*, **86**, 5914 (2014).
8. N. Radenahmad, A. Afif, P. I. Petra, S. M. Rahman, S.-G. Eriksson and A. K. Azad, *Renewable and Sustainable Energy Reviews*, **57**, 1347 (2016).
9. N. S. Nguyen, G. Das and H. H. Yoon, *Biosensors and Bioelectronics*, **77**, 372 (2016).
10. S. Zhan, Z. Zhou, M. Liu, Y. Jiao and H. Wang, *Catalysis Today*, **327**, 398 (2019).
11. D. Zhu, C. Guo, J. Liu, L. Wang, Y. Du and S.-Z. Qiao, *Chem Commun*, **53**, 10906 (2017).
12. V. K. Gupta, R. N. Goyal and R. A. Sharma, *Analytica Chimica Acta*, **647**, 66 (2009).
13. B. K. Boggs, R. L. King and G. G. Botte, *Chem Commun*, 4859 (2009).
14. Y. Velichkova, Y. Ivanov, I. Marinov, R. Ramesh, N. R. Kamini, N. Dimcheva, E. Horozova and T. Godjevargova, *Journal of Molecular Catalysis B: Enzymatic*, **69**, 168 (2011).
15. M. Nie, S. Du, Q. Li, M. Hummel, Z. Gu and S. Lu, *Journal of The Electrochemical Society*, **167**, 044510 (2020).
16. M. Nie, S. Lu, Q. Li, X. Liu and S. Du, *SCIENTIA SINICA Chimica*, **46**, 357.
17. V. K. Gupta, H. Karimi-Maleh and R. Sadegh, *Int. J. Electrochem. Sci*, **10**, 303 (2015).
18. V. K. Gupta, A. K. Singh and L. K. Kumawat, *Sensors and Actuators B: Chemical*, **195**, 98 (2014).
19. V. K. Gupta, S. Kumar, R. Singh, L. Singh, S. Shoora and B. Sethi, *Journal of Molecular Liquids*, **195**, 65 (2014).
20. M. H. Dehghani, D. Sanaei, I. Ali and A. Bhatnagar, *Journal of molecular liquids*, **215**, 671 (2016).
21. R. N. Goyal, V. K. Gupta, A. Sangal and N. Bachheti, *Electroanalysis: An International Journal Devoted to Fundamental and Practical Aspects of Electroanalysis*, **17**, 2217 (2005).
22. R. N. Goyal, V. K. Gupta and S. Chatterjee, *Biosensors and Bioelectronics*, **24**, 1649 (2009).
23. R. N. Goyal, V. K. Gupta and S. Chatterjee, *Biosensors and Bioelectronics*, **24**, 3562 (2009).
24. Z. Lin, W. Xue, H. Chen and J.-M. Lin, *Analytical Chemistry*, **83**, 8245 (2011).
25. L. J. Gimbert and P. J. Worsfold, *TrAC Trends in Analytical Chemistry*, **26**, 914 (2007).

26. M. C. Breadmore, A. I. Shallan, H. R. Rabanes, D. Gstoettenmayr, A. S. Abdul Keyon, A. Gaspar, M. Dawod and J. P. Quirino, *Electrophoresis*, **34**, 29 (2013).
27. J. Zhang, Z. Chen, H. Wu, F. Wu, C. He, B. Wang, Y. Wu and Z. Ren, *Journal of Materials Chemistry B*, **4**, 1310 (2016).
28. F. Bedioui and S. Griveau, *Electroanalysis*, **25**, 587 (2013).
29. R. Chokkareddy, G. G. Redhi and T. Karthick, *Heliyon*, **5**, e01457 (2019).
30. S. Lu, M. Hummel, S. Kang and Z. Gu, *J Electrochem Soc*, **167**, 046515 (2020).
31. S. Lu, M. Hummel, K. Chen, Y. Zhou, S. Kang and Z. Gu, *Electrochemistry Communications*, **114**, 106715 (2020).
32. M. Nie, S. Lu, D. Lei, C. Yang and Z. Zhao, *Journal of The Electrochemical Society*, **164**, H952 (2017).
33. T. A. Ahmed, G. Kulshreshtha and M. T. Hincke, in *Eggs as Functional Foods and Nutraceuticals for Human Health*, p. 359 (2019).
34. S. H. Chung and A. Manthiram, *Advanced Materials*, **26**, 1360 (2014).
35. S. Park, K. S. Choi, D. Lee, D. Kim, K. T. Lim, K.-H. Lee, H. Seonwoo and J. Kim, *Biosystems Engineering*, **151**, 446 (2016).
36. L. Huang, J. Li, Z. Wang, Y. Li, X. He and Y. Yuan, *Carbon*, **143**, 507 (2019).
37. X. Meng and D. Deng, *Chemical Engineering Science*, **194**, 134 (2019).
38. J. Zhao, J. A. Syed, X. Wen, H. Lu and X. Meng, *Journal of Alloys and Compounds*, **777**, 974 (2019).
39. S.-L. Zhong, J. Zhuang, D.-P. Yang and D. Tang, *Biosensors and Bioelectronics*, **96**, 26 (2017).
40. Z. Li, L. Zhang, B. S. Amirkhiz, X. Tan, Z. Xu, H. Wang, B. C. Olsen, C. M. Holt and D. Mitlin, *Advanced Energy Materials*, **2**, 431 (2012).
41. S. Lu, M. Hummel, Z. Gu, Y. Gu, Z. Cen, L. Wei, Y. Zhou, C. Zhang and C. Yang, *Int J Hydrogen Energ*, **44**, 16144 (2019).
42. L. Lu, *Sensors and Actuators B: Chemical*, **281**, 182 (2019).
43. S. Lu, C. Yang and M. Nie, *Journal of Alloys and Compounds*, **708**, 780 (2017).
44. S. Trasatti and O. Petrii, *Journal of Electroanalytical Chemistry*, **327**, 353 (1992).
45. R. M. Penner and C. R. Martin, *Analytical Chemistry*, **59**, 2625 (1987).
46. B. S. Yeo and A. T. Bell, *The Journal of Physical Chemistry C*, **116**, 8394 (2012).
47. L. Y. Zhang, Y. Ouyang, S. Wang, Y. Gong, M. Jiang, W. Yuan and C. M. Li, *Journal of Power Sources*, **447**, 227248 (2020).
48. H. D. Mai, G. Y. Sung and H. Yoo, *Rsc Adv*, **5**, 78807 (2015).
49. T. Ahuja, D. Kumar, N. Singh, A. M. Biradar and Rajesh, *Materials Science and Engineering: C*, **31**, 90 (2011).
50. M. Tyagi, M. Tomar and V. Gupta, *Biosensors and Bioelectronics*, **41**, 110 (2013).
51. C.-P. Huang, Y.-K. Li and T.-M. Chen, *Biosensors and Bioelectronics*, **22**, 1835 (2007).